Ideal strength of silicon: An *ab initio* study

S. M.-M. Dubois,[1,*] G.-M. Rignanese,[1,2] T. Pardoen,[2,3] and J.-C. Charlier[1,2]

[1]*Unité de Physico-Chimie et de Physique des Matériaux (PCPM), Université catholique de Louvain, Place Croix du Sud, 1 (Boltzmann)
B-1348 Louvain-la-Neuve, Belgium*
[2]*Research Center in Micro and Nanoscopic Materials and Electronic Devices (CERMIN),
Université catholique de Louvain B-1348 Louvain-la-Neuve, Belgium*
[3]*Unité d'Ingénierie des Matériaux et des Procédés (IMAP) Université catholique de Louvain, Place Sainte Barbe, 2 (Réaumur)
B-1348 Louvain-la-Neuve, Belgium*

The ideal strength of silicon is predicted along various loading paths using density functional theory. Stress-strain curves are calculated under uniaxial tension, relaxed shear, and uniaxial deformation conditions. In order to check the stability of the deformation paths, the phonon spectra and the stiffness tensors are computed within density-functional perturbation theory. A second-order phase transition is found to occur before the elastic instability when applying a $\{111\}\langle\bar{1}\ \bar{1}2\rangle$ relaxed shear. In all the other deformation conditions, the first predicted instabilities are located at the center of the Brillouin zone. Finally, the crystallographic nature of the instabilities is investigated by the calculation of the phonon eigendisplacements and by the decomposition of the stiffness tensors.

PACS number(s): 62.20.−x, 63.20.Dj, 71.15.Mb

I. INTRODUCTION

The ideal strength of a material is defined as the critical level of external stress under which a perfect, infinite homogeneous lattice becomes structurally unstable. It gives an upper limit on the stress that a material can sustain. Often, this upper limit is far beyond experiment reach due to the presence of defects in the material. However, stresses approaching the ideal strength have been measured in whiskers[1,2] or in nanoindentation experiments involving almost defect-free regions.[3] In addition, the ideal strength provides insight into the connections between the nature and symmetry of the crystal and its mechanical behavior. For instance, based on calculations of the ideal strength of diamond, an explanation was proposed for the dominance of the {111} cleavage plane in diamond.[4] More recently, it was found that shear failure is an inherent property of aluminum by analyzing its structural instabilities.[5] Finally, the theoretical values calculated on ideal structures can be used as input parameters for multiscale models.[6]

The mechanical stability of homogeneous crystals has been the subject of a long theoretical debate. Born initiated the systematic study of crystal stability, establishing a criterion in terms of the elastic constants.[7,8] During the last two decades, studies have been performed in order to generalize Born's work to strained states.[9–12] In particular, it was shown[12] that a homogeneously strained crystal remains stable with respect to elastic instabilities as long as the symmetric part of the stiffness tensor keeps its positiveness.[13]

However, in the past few years, stringent limitations of this criterion have been underlined. Several recent studies have shown that the ideal strength does not depend only on elastic instabilities.[5,14] Indeed, an instability related to a vibrational mode can also appear before the material becomes elastically unstable. These instabilities, also called inelastic or phonon instabilities, appear when a phonon mode lowers the energy of the crystal.[15] Indeed, when the energy of a

phonon becomes negative, its amplitude increases, and the induced distortion drives the system into another stable state. Stability requires thus that the relative energy of each phonon mode be positive over the entire Brillouin zone.[8,16] As the eigendisplacements corresponding to the different phonon modes form a complete basis set for all crystal distortions, the analysis of the complete phonon spectrum appears to be a necessary and sufficient stability criterion.

With the present development of MEMS and NEMS, the mechanical behavior of materials at the atomic scale is of great interest. Due to its technological importance, silicon has been intensively studied. However, the previous works on its ideal strength have essentially relied on stiffness tensor calculations.[17–19] It is also worth mentioning calculations of crack propagation in silicon on {111} cleavage planes.[20,21] In this paper, the possible limitation of the ideal strength of silicon by phonon instabilities is investigated using first-principles calculations. The stress-strain curves are calculated for uniaxial tension and uniaxial deformation along the $\langle 100 \rangle$ direction, which is of technological interest due to its use as preferential direction for epitaxial growth, the $\langle 110 \rangle$ and $\langle 111 \rangle$ directions which are the two principal cleavage planes. The same calculations are performed for relaxed shear on the {111} plane in the $\langle\bar{1}\ \bar{1}2\rangle$ and $\langle 1\bar{1}0\rangle$ directions which are two of the principal slip systems of silicon. The ideal strengths corresponding to these loading paths are estimated from both complete phonon spectra and stiffness tensors calculations. Finally, the nature of the instabilities is discussed.

II. TECHNICAL DETAILS

The calculations are performed on the silicon primitive cell containing two atoms. Total energies, stresses, dynamical matrices and elastic constants are calculated using density-functional theory[22,23] and the perturbation theory,[24,25]

TABLE I. Calculated and experimental lattice parameters, elastic constants, and Poisson's ratios (in the directions $\langle 100 \rangle$, $\langle 110 \rangle$ (Ref. 31), and $\langle 111 \rangle$) for Si. The reported Poisson's ratios are derived from the calculated elastic constants. The experimental values are taken from Ref. 32 for the lattice constant (at room temperature), from Ref. 33 for the elastic constants (at 77 K), and from Ref. 34 for the Poisson's ratios. The last column gives the relative deviation of the calculated values from the measured ones.

	Calculated	Experiment	% Deviation
a_0 (Bohr)	10.201	10.263	−0.6
c_{11} (GPa)	161.5	166	−2.7
c_{12} (GPa)	63.8	64	−0.3
c_{44} (GPa)	76.9	80	−3.8
$\nu_{\langle 100 \rangle}$	0.283	0.279	1.4
$\nu_{\langle 110 \rangle}$	0.369	0.368	0.3
$\nu_{\langle 111 \rangle}$	0.184	0.180	2.2

as implemented in the ABINIT code.[26] The exchange-correlation energy is evaluated within the local-density approximation using the Teter-Pade parametrization.[27] The interaction of the valence electrons with the ionic cores is represented with a separable, norm-conserving Troullier-Martins pseudopotential.[28] The wave functions are expanded into plane waves up to a cutoff energy of 10 hartrees. The Brillouin zone (BZ) integration is performed using a cold smearing technique[29] with a smearing parameter of 0.01 hartree. The convergence of the total energies and derivatives requires a $12 \times 12 \times 12$ Monkhorst-Pack k-point grid.[30] The remaining error on the stresses due to the smearing parameter, finite basis set, and k-point sampling is estimated to be lower than ~ 0.05 GPa. With the parameters above, the calculated lattice parameters, elastic constants, and Poisson's ratios of Si are found to be in good agreement with the experimental ones, as reported in Table I.

The computation of the ideal strength is achieved in two steps. First, the unrelaxed stress-strain curves are calculated by straining the crystal with a series of increments and allowing only for the relaxation of the relative atomic positions (the lattice vectors are kept fixed). Using a system of Cartesian coordinates, the imposed strain components can be expressed in dyadic form as

$$\boldsymbol{\epsilon}_{tension} = \boldsymbol{\epsilon}_{11}(\underline{e}_1 \otimes \underline{e}_1), \quad (1)$$

where $\underline{e}_1$ is a unit vector in the tension direction, and,

$$\boldsymbol{\epsilon}_{shear} = \boldsymbol{\epsilon}_{31}(\underline{e}_3 \otimes \underline{e}_1), \quad (2)$$

where $\underline{e}_1$ and $\underline{e}_3$ are unit vectors respectively perpendicular to the shear plane and in the direction of shear. In such a non-fully-relaxed configuration, large transverse stresses generally appear. The fully relaxed loading path is thus obtained by performing, at each incremental strain, a relaxation of both the lattice vectors and the atomic relative positions in order to cancel the components of the stress tensor orthogonal to the applied strain. In this way, we are able to simulate uniaxial tension and relaxed shear conditions (see Fig. 1).
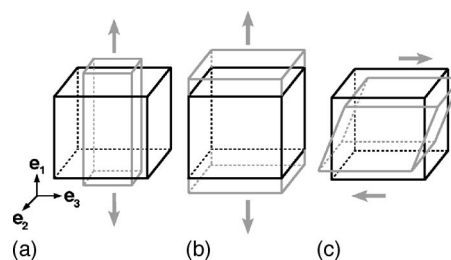

FIG. 1. Schematic representation of the loading conditions. (a) Uniaxial tension (fully relaxed tension); (b) uniaxial deformation (unrelaxed tension); (c) relaxed shear.

Using the same Cartesian coordinates as before, the stress tensors may then be expressed as

$$\boldsymbol{\sigma}_{tension} = \sigma_{11}(\underline{e}_1 \otimes \underline{e}_1) \quad \text{and} \quad \boldsymbol{\sigma}_{shear} = \sigma_{31}(\underline{e}_3 \otimes \underline{e}_1). \quad (3)$$

In practice, the relaxation is stopped when the undesired stress components become less than 0.02 GPa.

Second, for each loading path, the crystal stability is analyzed using stiffness tensors decomposition and complete phonon spectra calculation. Stiffness tensors are obtained on the basis of the calculated stresses and elastic constants.[13] Using Kelvin notation and spectral theory,[35,36] the stiffness tensor is then decomposed and the crystallographic nature of the instabilities is analyzed. Phonon energies over the whole
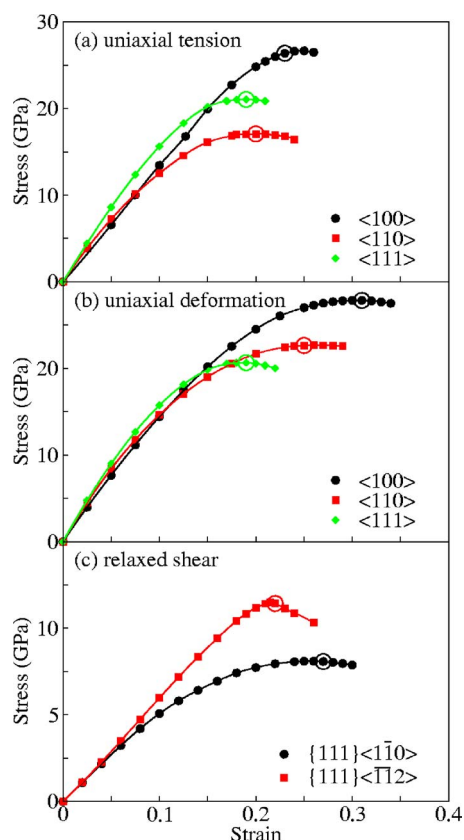

FIG. 2. (Color online) Stress-strain relations for various loading paths (as indicated in key). The open ring indicates the first appearance of an unstable phonon mode along each path.

TABLE II. Calculated ideal tensile strength of Si and associated engineering strain.

	Computed values		Previous works	
	Stress (GPa)	Engineering strain (%)	Stress (GPa)	Engineering strain (%)
$\langle 100 \rangle$ uniaxal tension	26.4	23	10.7[a]	9.4[a]
$\langle 110 \rangle$ uniaxal tension	17.0	20		
$\langle 111 \rangle$ uniaxal tension	21.0	19	22.0[b]	17[b]
$\langle 100 \rangle$ uniaxal deformation	27.8	31		
$\langle 110 \rangle$ uniaxal deformation	22.6	25		
$\langle 111 \rangle$ uniaxal deformation	20.7	19		
$\{111\}\langle \bar{1}\,\bar{1}2 \rangle$ shear	11.4	22.0	6.8[b]	30.0[b]
$\{111\}\langle 1\bar{1}0 \rangle$ shear	8.0	27.0	9.6[c]	27[c]

[a]From Ref. 18.
[b]From Ref. 17.
[c]From Ref. 19.

Brillouin zone are obtained by interpolating the dynamical matrix calculated on a $6 \times 6 \times 6$ q-point grid. In the directions of high symmetry which present unstable phonon modes, the phonon energies are recalculated explicitly in order to avoid interpolation errors. Finally, on the basis of the eigendisplacement calculation, the crystallographic nature of the instabilities is analyzed. Moreover, for vanishing wavelengths, the eigendisplacements can be described to first order by a homogeneous deformation whose deformation parameters are given by[37]

$$\mu_{\alpha\beta} = \text{Re}\{2\pi i q_\beta u_\alpha\}, \qquad (4)$$

where $\boldsymbol{q}$ is the wavelength and $\boldsymbol{u}$ is the limit of the eigendisplacements for vanishing wavelengths.

III. RESULTS

A. The stress-strain curves

The first step in the estimation of the ideal strength is the calculation of the deformation path. The stress-strain curves obtained for Si along the eight investigated paths are reported in Fig. 2. The open circles on these curves indicate the states for which the first instability has been detected using the phonon-based criterion.

As expected, the curves corresponding to shear show stresses lower than those related to tension. Indeed, shear moduli are always lower than tension moduli. Moreover, it appears that shear is easier in the $\langle 1\bar{1}0 \rangle$ direction. As far as tension is concerned, the maximum stresses vary significantly with the loading direction. Indeed, the maximum along $\langle 100 \rangle$ is far above those obtained along $\langle 110 \rangle$ and $\langle 111 \rangle$. This is not very surprising in view of experimental works that have identified the $\{110\}$ and $\{111\}$ planes as the two principal cleavage planes of silicon.[38,39] Finally, it appears that, along the $\langle 111 \rangle$ direction, the stresses are not affected by transverse relaxation. This is clearly not the case along the $\langle 100 \rangle$ and $\langle 110 \rangle$ directions for which the stress-strain responses expand to larger strain and stress, respec-

tively, for unrelaxed tension. The Poisson's ratios of silicon, reported in Table I, for the three loading directions studied underline the poor effect of the transverse relaxation in the case of the $\langle 111 \rangle$ tension. Moreover, the value of the $\langle 111 \rangle$ Poisson's ratio is found to be similar in other zinc-blende materials like Ge,[34] GaAs,[40] and BN.[41] This specific behavior along the $\langle 111 \rangle$ tension direction seems thus to be related to the close-packed nature of the $\{111\}$ planes.

B. The ideal strength

We now focus on the states corresponding to the onset of the instability. In all the investigated loading path except for the $\{111\}\langle \bar{1}\,\bar{1}2 \rangle$ relaxed shear, the calculations of the complete phonon spectra show that the first unstable modes have a zone center wave vector, implying that they correspond to elastic instabilities. As expected, the criterion based on the stiffness tensor gives the same results. In practice, the agreement between the two criteria is better than 1% of strain, which is very good.

TABLE III. Crystallographic nature of the first appearing instability for each loading path.

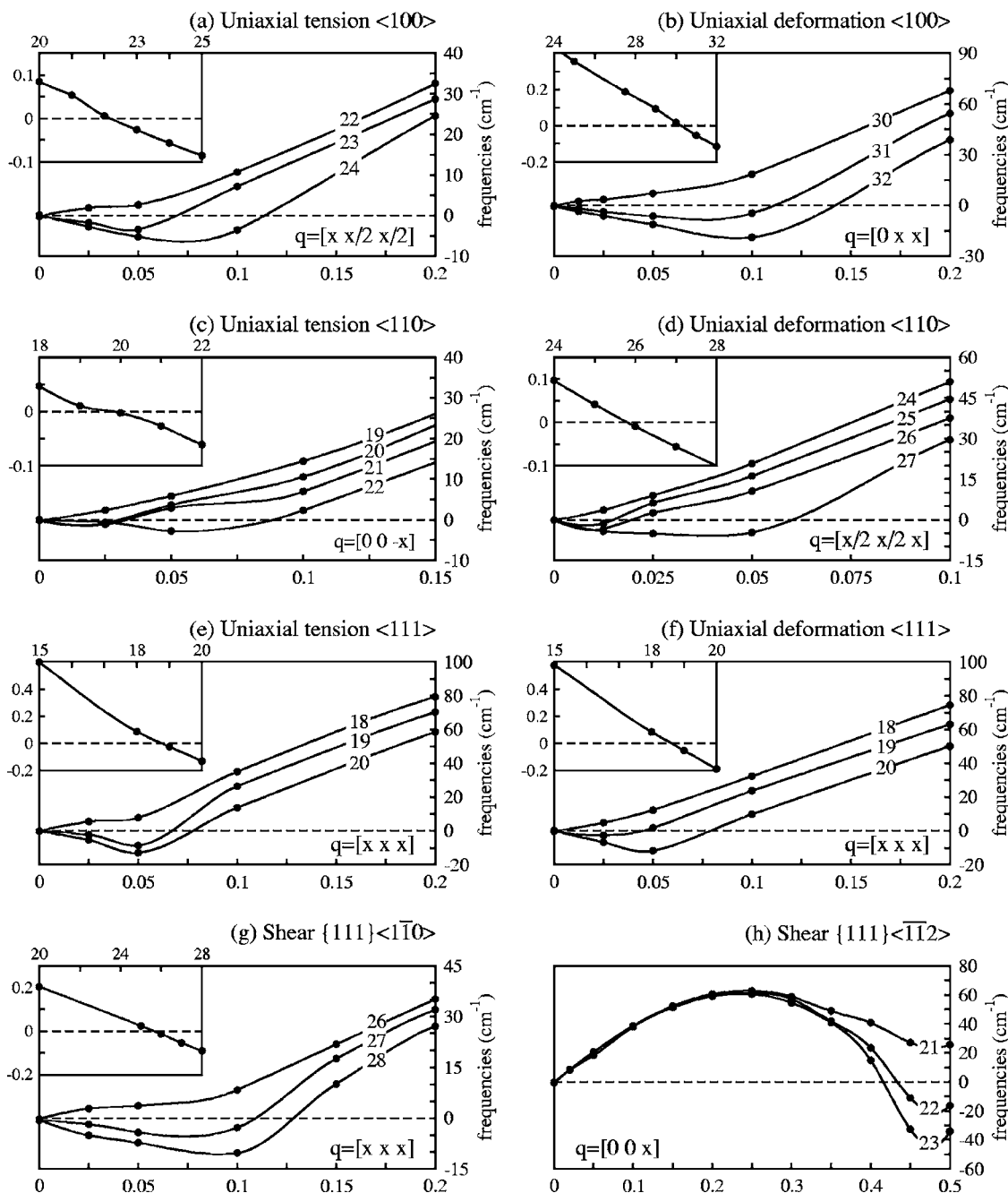|	Nature of the instability
$\langle 100 \rangle$ uniaxal tension	$\{011\}\langle 01\bar{1} \rangle$ shear
	$\{111\}\langle \bar{1}\bar{1}2 \rangle$ shear
$\langle 110 \rangle$ uniaxal tension	$\{\bar{1}\bar{1}1\}\langle 112 \rangle$ shear
$\langle 111 \rangle$ uniaxal tension	$\langle 111 \rangle$ tension
$\langle 100 \rangle$ uniaxal deform.	$\langle 100 \rangle$ tension
$\langle 110 \rangle$ uniaxal deform.	$\langle 110 \rangle$ tension
$\langle 111 \rangle$ uniaxal deform.	$\langle 111 \rangle$ tension
$\{111\}\langle 1\bar{1}0 \rangle$ shear	$\{111\}\langle 1\bar{1}0 \rangle$ shear
$\{111\}\langle \bar{1}\,\bar{1}2 \rangle$ shear	$\{111\}\langle \bar{1}\,\bar{1}2 \rangle$ shear

FIG. 3. Phonon energies along the direction of the first reported instability for various strains, for each of the investigated deformation conditions. The directions are indicated by their wave vector q given in reciprocal coordinates by multiples of the x coordinate of the plot. The level of strain is indicated as a percentage on the curve. The stiffness tensor eigenvalue (given in units of 100 GPa) corresponding to the phonon mode as a function of strain (in %) are reported in insets. Lines come from spline interpolation of the calculated results.

The case of the $\{111\}\langle\bar{1}\,\bar{1}2\rangle$ relaxed shear is quite different. Indeed, for a deformation of 22% a phonon instability occurs before the crystal becomes elastically unstable. This phonon mode induces a second-order phase transition which limits the $\{111\}\langle\bar{1}\,\bar{1}2\rangle$ shear strength of silicon. This transition cannot be detected based on the stiffness criterion.

The computed values for the ideal strength of silicon are collected in Table II together with values from previous works. We note that the computed ideal strength along the

relaxed $\langle111\rangle$ is in good agreement with the results of Roundy and Cohen.[17] Conversely, significant discrepancies are observed when comparing our results with the values obtained by Yashiro *et al.*[18] Their stress-strain curves along the relaxed $\langle001\rangle$ loading path might not be fully converged due to insufficient k-point sampling of the BZ. For silicon in shear, we note a good agreement between the computed $\{111\}\langle1\bar{1}0\rangle$ shear strength and the results obtained by Ogata *et al.*,[19] but we cannot explain the divergence with the result
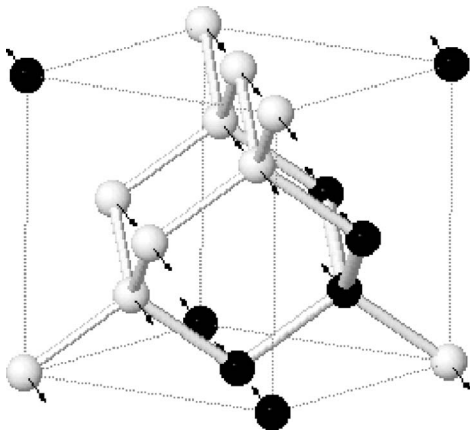
FIG. 4. Representation of the atomic displacements inducing the phase transition when a $\{111\}\langle\bar{1}\,\bar{1}2\rangle$ relaxed shear is applied to the silicon structure.

of Roundy and Cohen[17] concerning the $\{111\}\langle\bar{1}\,\bar{1}2\rangle$ direction. However, experimentally the $\langle1\bar{1}0\rangle$ direction is found to be the easiest propagation direction for cleavage in silicon, which tends to support our results.[38]

C. The crystallographic nature of the instabilities

For a given loading path, the crystallographic nature of the instability can be investigated either by the spectral decomposition of the corresponding stiffness tensor or by introducing the atomic eigendisplacements in Eq. (4). In principle, when the ideal strength is limited by the appearance of an elastic instability (which is the case for most of the loading paths studied), these two methods should give the same results. In practice, the eigenvectors of the stiffness tensor expressed in the Kelvin notation are found to match almost perfectly the strain tensors obtained with Eq. (4). The crystallographic nature of the instabilities is summarized in Table III.

The phonon energies along the directions of the BZ where the first unstable phonon mode has been localized are reported in Fig. 3 for various strains around the critical value. The stiffness tensor eigenvalues corresponding to these unstable phonon modes are also reported in Fig. 3 as insets. As indicated previously, the two criteria appear to be in good agreement.

For uniaxial tension along $\langle100\rangle$ [Fig. 3(a)], the first instability arises for a strain equal to $\sim23\%$. The calculation of the eigendisplacements indicates a $\{011\}\langle01\bar{1}\rangle$ shear instability. A second instability associated to $\{111\}\langle\bar{1}\,\bar{1}2\rangle$ shear arises at $\sim25\%$ strain. This instability is not shown on the graph for reasons of clarity. For uniaxial deformation along $\langle100\rangle$ [Fig. 3(b)], the crystal becomes unstable with respect to the applied $\langle100\rangle$ tensile strain for a deformation equal to $\sim31\%$. For uniaxial tension along $\langle110\rangle$ [Fig. 3(c)], the elastic instability appearing at $\sim20\%$ of deformation can be associated to a $\{\bar{1}\,\bar{1}1\}\langle112\rangle$ shear strain. For uniaxial deformation [Fig. 3(d)], the crystal becomes unstable with respect to
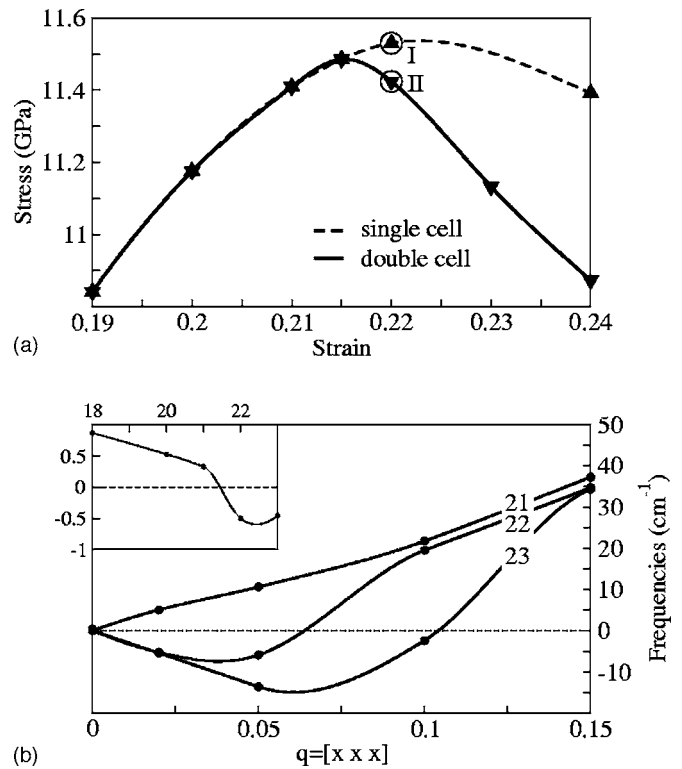

FIG. 5. (a) Comparison of the $\{111\}\langle\bar{1}\,\bar{1}2\rangle$ relaxed shear loading path calculated with a single and a double unit cell. When working with the single cell (dashed curve), a phonon instability is detected (point I); while, with the double cell (solid curve), the first instability to occur (point II) is elastic. (b) Phonon energies calculated at point II along the direction of instability, as a function of strain (lines come from spline interpolation of the calculated results).

the applied $\langle110\rangle$ tensile strain. Hence, the presence of transverse stresses tends to favor this tensile instability rather than the $\{\bar{1}\,\bar{1}1\}\langle112\rangle$ shear instability probably by decreasing of the maximum shear stress. For uniaxial tension and deformation along $\langle111\rangle$ [Figs. 3(e) and 3(f)], the instabilities are found to correspond to the applied $\langle111\rangle$ tensile strain. This is not surprising due to limited effect of the lattice relaxation along the $\langle111\rangle$ loading path. For $\{111\}\langle1\bar{1}0\rangle$ relaxed shear [Fig. 3(g)], the elastic instability is associated to a $\{111\}\times\langle1\bar{1}0\rangle$ shear strain. For $\{111\}\langle\bar{1}\,\bar{1}2\rangle$ relaxed shear [Fig. 3(h)], the first appearing instability results from an unstable phonon at the border of the BZ. In this case, the crystallographic nature of the instability is no longer a homogeneous deformation. Indeed, by doubling the unit cell in the $\langle001\rangle$ direction and relaxing the atomic positions, it appears clearly that the instability corresponds to a second order phase transition. The atomic displacements associated with this phase transition are described in Fig. 4. The neighboring $\{\bar{1}\,\bar{1}1\}$ atomic planes (indicated by a black and white coloring of the atoms) glide along the $\langle\bar{1}10\rangle$ in opposite directions, suggesting that the phase transition involves mainly a shear component.

Moreover, a new loading path has to be considered beyond the transition. As illustrated in Fig. 5(a), when using

single cell, an unstable phonon appears at point I. Conversely, with the double cell, the crystal evolves toward a new state, labeled by point II, where stresses are lowered. Consequently, the phase transition reduces the ideal strength along this peculiar direction. Finally, the crystal stability has been investigated along this new loading path and an elastic instability has been located for a deformation of ~22% [Fig. 5(b)]. The latter instability can be associated with a {111} $\times \langle \bar{1}\,\bar{1}2 \rangle$ shear.

IV. CONCLUSIONS

The ideal tensile strength of silicon has been calculated for various loading paths. The crystallographic nature of the corresponding first instabilities has also been analyzed. Our calculations reveal that for most loading paths, the instability responsible for crystal failure is elastic.

As expected in such situations, the ideal strength deduced from the analysis of the elastic stability of the crystal corresponds exactly to the one obtained by complete phonon spectra inspection. Moreover, the crystallographic nature of the

instabilities deduced from the phonon eigendisplacements and from the stiffness tensors are found to be the same.

This work suggests that at least two shear systems, {111}⟨1$\bar{2}$1⟩ and {110}⟨1$\bar{1}$0⟩, are responsible for the limitation of the ideal strength of silicon. However, along the {111} $\times \langle \bar{1}\,\bar{1}2 \rangle$ relaxed shear, an unstable phonon mode has been located away from the center of the BZ. This phonon is associated with a second-order phase transition.

ACKNOWLEDGMENTS

*Electronic address: sdubois@pcpm.ucl.ac.be

[1] S. S. Brenner, J. Appl. Phys. **27**, 1484 (1956).

[2] A. Kelly and N. H. Macmillan, *Strong Solids* (Clarendon, Oxford, 1986).

[3] C. R. Krenn, D. Roundy, M. L. Cohen, D. C. Chrzan, and J. W. Morris Jr., Phys. Rev. B **65**, 134111 (2002).

[4] R. H. Telling, C. J. Pickard, M. C. Payne, and J. E. Field, Phys. Rev. Lett. **84**, 5160 (2000).

[5] D. M. Clatterbuck, C. R. Krenn, M. L. Cohen, and J. W. Morris Jr., Phys. Rev. Lett. **91**, 135501 (2003).

[6] A. Van der Ven and G. Ceder, Acta Mater. **52**, 1223 (2003).

[7] M. Born, Proc. Cambridge Philos. Soc. **36**, 160 (1940).

[8] M. Born and K. Huang, *Dynamical Theory of Crystal Lattices* (Clarendon, Oxford, 1954), pp. 129–165.

[9] Z. Zhou and B. Joós, Phys. Rev. B **54**, 3841 (1996).

[10] J. W. Morris Jr., and C. R. Krenn, Philos. Mag. A **80**, 2827 (2000).

[11] J. Wang, S. Yip, S. R. Phillpot, and D. Wolf, Phys. Rev. Lett. **71**, 4182 (1993).

[12] J. Wang, J. Li, S. Yip, S. Phillpot, and D. Wolf, Phys. Rev. B **52**, 12627 (1995).

[13] For the sake of completeness, we provide here the definition of the stiffness tensor $\mathring{c}_{\alpha\beta\sigma\tau}$ introduced in Refs. 9 and 12. For a homogeneous crystal in the $\mathring{\Omega}$ configuration for which the applied uniform stress is $\mathring{S}_{\alpha\beta}$, the crystal volume is $\mathring{V}$, and the internal energy is $\mathring{U}$, the stiffness tensor is given by

$$\mathring{c}_{\alpha\beta\sigma\tau}(\mathring{\Omega}) = \mathring{C}_{\alpha\beta\sigma\tau}(\mathring{\Omega}) + (1/2)(\delta_{\alpha\sigma}\mathring{S}_{\beta\tau} + \delta_{\beta\sigma}\mathring{S}_{\alpha\tau} + \delta_{\alpha\tau}\mathring{S}_{\beta\sigma} + \delta_{\beta\tau}\mathring{S}_{\alpha\sigma} - 2\delta_{\sigma\tau}\mathring{S}_{\alpha\beta}),$$

where $\eta_{\alpha\beta}$ is a virtual Lagrangian strain which would bring the crystal into the configuration Ω, where the volume would be V and the internal energy U. $\delta_{\alpha\beta}$ is the identity matrix, and $\mathring{C}_{\alpha\beta\sigma\tau}$

is

$$\mathring{C}_{\alpha\beta\sigma\tau}(\mathring{\Omega}) = \frac{1}{\mathring{V}} \left(\frac{\partial^2 U(\Omega)}{\partial \eta_{\alpha\beta}\,\partial\,\eta_{\sigma\tau}} \right)\Bigg|_{\mathring{\Omega}}.$$

[14] S.-H. Jhi, S. G. Louie, M. L. Cohen, and J. W. Morris Jr., Phys. Rev. Lett. **87**, 075503 (2001).

[15] In the present paper, we restrict the concept of phonon instability to the unstable phonon modes with nonvanishing wave vectors. Indeed, the elastic instabilities may be interpreted in terms of phonons with vanishing wave vectors [see M. Born and K. Huang, *Dynamical Theory of Crystal Lattices* (Clarendon, Oxford, 1954), pp. 229–236].

[16] D. C. Wallace, *Thermodynamics of Crystals* (Wiley, New York, 1972), pp. 32–41.

[17] D. Roundy and M. L. Cohen, Phys. Rev. B **64**, 212103 (2001).

[18] K. Yashiro, M. Oho, and Y. Tomita, Comput. Mater. Sci. **29**, 397 (2004).

[19] S. Ogata, J. Li, N. Hirosaki, Y. Shibutani, and S. Yip, Phys. Rev. B **70**, 104104 (2004).

[20] T. Zhu, J. Li, and S. Yip, Phys. Rev. Lett. **93**, 205504 (2004).

[21] R. Pérez and P. Gumbsch, Acta Mater. **48**, 4517 (2000).

[22] O. H. Nielsen and R. M. Martin, Phys. Rev. B **32**, 3792 (1985).

[23] D. M. Bylander, L. Kleinman, and S. Lee, Phys. Rev. B **42**, 1394 (1990).

[24] S. Baroni, P. Giannozzi, and A. Testa, Phys. Rev. Lett. **58**, 1861 (1987).

[25] X. Gonze and J.-P. Vigneron, Phys. Rev. B **39**, 13120 (1989).

[26] X. Gonze, J.-M. Beuken, R. Caracas, F. Detraux, M. Fuchs, G.-M. Rignanese, L. Sindic, M. Verstraete, G. Zerah, F. Jollet, M. Torrent, A. Roy, M. Mikami, Ph. Ghosez, J.-Y. Raty, and D. C. Allan, Comput. Mater. Sci. **25**, 478 (2002).

[27] See appendix of S. Goedecker, M. Teter, and J. Hutter, Phys. Rev. B **54**, 1703 (1996).

[28] N. Troullier and J. L. Martins, Phys. Rev. B **43**, 1993 (1991).

[29] N. Marzari, Ph.D. thesis, Cambridge University, 1996.

[30] H. J. Monkhorst and J. D. Pack, Phys. Rev. B **13**, 5188 (1976).

[31] The Poisson's ratio $\nu_{\langle 110 \rangle}$ does not show a cylindrical symmetry. In this case, the reported values are taken along the $\langle 001 \rangle$ direction.

[32] G. Basile, A. Bergamin, G. Cavagnero, G. Mana, E. Vittone, and G. Zosi, Phys. Rev. Lett. **72**, 3133 (1994).

[33] G. Simmons and H. Wang, *Single Crystal Elastic Constants and Calculated Aggregate Properties: A Handbook* (MIT Press, Cambridge, MA, 1971).

[34] J. J. Wortman and R. A. Evans, J. Appl. Phys. **36**, 153 (1965).

[35] S. C. Cowin and M. M. Mehrabadi, J. Mech. Phys. Solids **40**, 1549 (1992).

[36] S. Sutcliffe, J. Appl. Mech. **59**, 762 (1992).

[37] This formula is derived from Eq. 26.21 of M. Born and K. Huang, *Dynamical Theory of Crystal Lattices* (Clarendon, Oxford, 1954), in the limit of vanishing wave vector.

[38] A. George and G. Michot, Mater. Sci. Eng., A **164**, 118 (1993).

[39] G. Michot, Cryst. Prop. Prep. **17-18**, 55 (1988).

[40] R. I. Cottam and G. A. Saunders, J. Phys. C **6**, 2105 (1973).

[41] M. Grimsditch and E. S. Zouboulis, J. Appl. Phys. **76**, 832 (1994).